Escape and spreading properties of charge-exchange resonances in ^{208}Bi

G. Colò and N. Van Giai
Division de Physique Théorique, Institut de Physique Nucléaire, 91406 Orsay Cedex, France

P.F. Bortignon
Dipartimento di Fisica, Università degli Studi,
and Istituto Nazionale di Fisica Nucleare, Sezione di Milano, Via Celoria 16, 20133 Milano, Italy

R.A. Broglia
Dipartimento di Fisica, Università degli Studi,
and Istituto Nazionale di Fisica Nucleare, Sezione di Milano, Via Celoria 16, 20133 Milano, Italy,
and Niels Bohr Institute, University of Copenhagen, 2100 Copenhagen, Denmark
(Received 22 April 1994)

The properties of charge-exchange excitations of ^{208}Pb with $\Delta L = 0$, i.e., the isobaric analog and Gamow-Teller resonances, are studied within a self-consistent model making use of an effective force of the Skyrme type. The well-known isobaric analog case is used to assess the reliability of the model. The calculated properties of the Gamow-Teller resonance are compared with recent experimental measurements with the aim of better understanding the microscopic structure of this mode.
PACS number(s): 21.60.Jz, 24.30.Cz, 25.55.Kr

I. INTRODUCTION

Giant resonances can be described as coherent superpositions of particle-hole excitations and their particle decays into given hole channels provide insight about the corresponding particle-hole amplitudes. Thus, the study of decay properties is a unique way to test model predictions for the resonance wave function. Experimental studies have recently been made of the particle decay properties of giant resonances by means of exclusive measurements where inelastically scattered projectiles, or light products of transfer reactions, are detected in coincidence with nucleons emitted by giant resonances of the target system. The corresponding results provide severe tests for the theoretical models.

The Gamow-Teller resonance (GTR) is the manifestation of the spin-isospin nuclear zero sound. This mode was predicted theoretically as the mechanism for explaining the missing strength in the decay of β-radioactive nuclei [1]. Its subsequent observation in (p,n) reactions has opened an important chapter of the historical development of experimental study of giant resonances when the availability of higher energy projectiles in the early 1980s led to the realization of reaction conditions under which spin-isospin modes can optimally be excited [2]. A first experiment aimed to study the proton decay of the GTR was performed in Groningen, and reported in Ref. [3]. The results of this measurement raised a number of questions, as they seemed to imply a vanishing spreading width for the GTR, which seems quite unlikely.

Renewed interest in the study of the properties of the GTR is indeed testified by two recent measurements, with different characteristics, at Osaka and MSU. The proton decay of the resonance in ^{208}Bi has been investigated, and in the Osaka experiment [4], the results appear in modest agreement with previous theoretical estimates given in Refs. [5,6], whereas preliminary indications from the MSU experiment seem to give a somewhat different result [7]. This has motivated the present work, in which we apply to the charge-exchange modes a model of giant resonances which includes in a self-consistent way the coupling mechanisms leading to the damping of these modes. This model has been already used to study the properties of the isoscalar giant monopole resonance in ^{208}Pb [8].

We have first concentrated, as a test case, on the isobaric analog resonance (IAR) in the nucleus ^{208}Bi where the data provides a clear picture of the resonance properties. The IAR would be degenerate with its isobaric multiplet partner, the ground state of ^{208}Pb, if the nuclear Hamiltonian were completely charge-independent. The energy difference, due mainly to Coulomb effects, has been studied over a long period of time and it is accurately known. The width of the IAR is known to be very small. This is because it has the same isospin as the parent state while surrounding states have the isospin of the ground state of ^{208}Bi, which differs by one unit. Consequently, they couple only weakly with the IAR. Thus, excitation energy and width of this resonance provide a stringent test for any theoretical model of charge-exchange collective states.

We shall show how this test has been passed by our model in Sec. IV, while the predictions associated with the GTR are presented in Sec. V. Conclusions are drawn in Sec. VI. Before this, we discuss in Sec. II the general features of the model already applied to other collective modes [8] while more specific considerations relevant to charge-exchange modes are made in Sec. III. Detailed expressions for the Hamiltonian matrix and decay branching ratios are given in Appendixes A and B.

II. GENERAL FORMALISM

The random phase approximation (RPA) provides, as a rule, an accurate description of the centroid of giant resonances and the fraction of the energy weighted sum rule (EWSR) exhausted by the mode. However, it is necessary to go beyond this approximation scheme in order to explain the damping properties of the collective motion. Indeed, giant resonances are known experimentally to have an energy width and therefore, a finite lifetime. A general theory of the resonance width can be found, e.g., in Refs. [9, 10], and a list of references of much of the theoretical work carried out during the last decade can be found in [11]. In many of these calculations parameters were adjusted at various steps of the computational procedure in order to fit experimental data. In what follows we present a model in which a phenomenological effective interaction of the Skyrme type is used as the starting point but after this *no further tuning of the parameters* is introduced up to final results.

We start by solving the Hartree-Fock (HF) set of equations for a given nucleus (A, Z) using a Skyrme two-body interaction [12]. A set of occupied single-particle levels is then obtained, as well as a self-consistent mean field, which is then diagonalized on a basis made up with harmonic oscillator wave functions. This diagonalization procedure can also be replaced by solving the HF mean field with a box boundary condition. It provides a discrete set of occupied and unoccupied levels, many of which are at positive energy. The quasibound levels belong to this set. After choosing a convenient cutoff—details about numerical procedures are given in Sec. III—a finite set of occupied and unoccupied levels labeled by $|i\rangle$ is determined. In the following, we denote the corresponding energies and wave functions by ε_i and φ_i [the radial part of the wave function will be expressed as $u_i(r)$].

Let us call Q_1 the subspace of nuclear configurations made up with the HF ground state and all the possible one particle-one hole (1p-1h) excitations built within the set $|i\rangle$. We shall denote by the same symbol subspaces and projectors onto them. Now, the nuclear Hamiltonian can be written as

$$H = H_0 + V_{ph}, \tag{2.1}$$

where H_0 is the HF Hamiltonian and V_{ph} is the particle-hole (p-h) interaction determined as the functional derivative of the self-consistent mean field with respect to the density. The usual Tamm-Dancoff approximation (TDA) or RPA in a discrete particle-hole space amount to solve TDA or RPA equations using the Hamiltonian Q_1HQ_1.

As said above, giant resonances are known to have a decay width, and we can distinguish two main mechanisms which give rise to it. The energy of the vibrational nuclear motion can be transferred out of the system by an escaping nucleon[1], or can be distributed among internal degrees of freedom giving rise to more complicated configurations than the initial configuration. The contributions to the width coming from these two damping effects are usually called, respectively, escape ($\Gamma^{\uparrow}$) and spreading ($\Gamma^{\downarrow}$) width. We must also mention another source of broadening of the line width, namely the Landau spreading which already appears at the level of discrete RPA or TDA calculations.

In order to account for escape and spreading effects, we build two other subspaces P and Q_2. The space P is made up with particle-hole configurations where the particle is in an unbound state, orthogonal to all states $|i\rangle$. To determine these unbound states, we use the following procedure. At positive energy ε we solve, for each partial wave $c \equiv (l, j)$, the radial scattering equation for H_0, projected on the orthogonal complement of set $|i\rangle$. We can thus ensure that the resulting outgoing wave functions $u^{(+)}_{c,\varepsilon}$ have no overlap with any of the states $|i\rangle$, i.e., P and Q_1 are orthogonal subspaces (for details, see [13–15]). The states $u^{(+)}_{c,\varepsilon}$ have no resonant behavior since quasibound states are among the states $|i\rangle$.

The space Q_2 is built with a set of "doorway states," the first step in the coupling of the ordered resonance motion with the compound nuclear states, in which energy is distributed among all degrees of freedom in a statistical way. We denote these "doorway states" by $|N\rangle$. As a first approximation we can think of them as formed by 2p-2h configurations, but we discuss later a more physical choice of them in terms of states made up with one of the 1p-1h excitations coupled to a collective vibration.

We decompose the nuclear Green's function G as a sum of terms like $Q_1GQ_1 + Q_1GP + \cdots$. Using the technique described in [10] one can show that by virtue of the equations of motion in the different subspaces and the properties of projectors, the Green's function Q_1GQ_1 obeys an equation where the effective Hamiltonian, after truncation of higher order couplings, is

$$\mathcal{H}(\omega) \equiv Q_1HQ_1 + W^{\uparrow}(\omega) + W^{\downarrow}(\omega) = Q_1HQ_1 + Q_1HP\frac{1}{\omega - PHP + i\epsilon}PHQ_1 + Q_1HQ_2\frac{1}{\omega - Q_2HQ_2 + i\epsilon}Q_2HQ_1, \tag{2.2}$$

where ω is the excitation energy. This energy-dependent, complex Hamitonian allows to work inside the space Q_1. It has complex eigenvalues whose imaginary parts originate from coupling to unbound and to more complicated configurations and give rise to escape and spreading widths.

The escape term $W^{\uparrow}(\omega)$ can be more easily evaluated if one replaces the complete Hamiltonian H by the one-body part H_0. The neglect of matrix elements of $Q_1V_{ph}P$ should be, in the present case, rather safe since discrete and continuum wave functions are essentially restricted to different radial intervals while V_{ph} interaction has zero range. In this approximation, the escape term can be

[1] Also a γ-ray can escape when selection rules allow it. In what follows we neglect this decay channel as it gives a minor contribution to the total width of the mode.

written [13] as

$$W^{\uparrow}(\omega) = \omega - H_0 - K, \tag{2.3}$$

where K is the inverse inside subspace Q_1 of the Green's function containing only the mean field Hamiltonian. This Green's function can be easily computed and inverted as it has only one-body matrix elements whereas taking into account the two-body interaction would have resulted in a much harder task. Detailed expressions are given in Appendix A. The accuracy of the procedure has been checked in [16], where the results obtained for the isoscalar monopole strength distribution in ^{40}Ca, by using the approximate $W^{\uparrow}$ of (2.3), were compared with those of exact continuum-RPA calculations and excellent agreement between the two calculations was found (see Fig. 1 of [16]). Yoshida and Adachi made a similar comparison in [14] and they concluded also that a good agreement can be obtained, provided a sufficiently large basis is employed (see Figs. 1–3 of [14]).

The matrix elements on a basis of Q_1 can also be determined in a straightforward way for the spreading term $W^{\downarrow}(\omega)$. We make the ansatz that the configurations $|N\rangle$ of Q_2 are not interacting[2]. This is reasonable since coupling among doorway states will correct the coupling between 1p-1h states and doorway states in higher order of the residual interaction. If we take a basis of p-h configurations, i.e., a set $|ph\rangle$ (particle levels are labeled by $p, p' \ldots$, and hole levels by $h, h' \ldots$), then the generic matrix element turns out to be

$$W^{\downarrow}_{ph,p'h'}(\omega) = \sum_N \frac{\langle ph|V|N\rangle\langle N|V|p'h'\rangle}{\omega - \omega_N}, \tag{2.4}$$

where we have omitted the subscript ph of the interaction, and ω_N is the energy of the state $|N\rangle$, in mean field approximation. Further clarifications about the evaluation of (2.4) are given in Sec. III.

It is found convenient, in order to solve the effective Hamiltonian (2.2), to work on the basis of the RPA or TDA states obtained by diagonalizing its first term. Using this basis, we provide explicit formulas for the matrix elements of the escape and spreading terms in Appendix A. In this matrix form, the eigenvalue equation for the effective Hamiltonian (2.2) is

$$\begin{pmatrix} \mathcal{D} + \mathcal{A}_1(\omega) & \mathcal{A}_2(\omega) \\ \mathcal{A}_3(\omega) & -\mathcal{D} + \mathcal{A}_4(\omega) \end{pmatrix} \begin{pmatrix} F^{(\nu)} \\ \bar{F}^{(\nu)} \end{pmatrix} = \left(\Omega_\nu - i\frac{\Gamma_\nu}{2}\right) \begin{pmatrix} F^{(\nu)} \\ \bar{F}^{(\nu)} \end{pmatrix}, \tag{2.5}$$

where $\mathcal{D}$ is a diagonal matrix with the RPA eigenvalues, and the $\mathcal{A}_i$ matrices which are energy dependent contain the escape and spreading contributions, as explained in Appendix A. We have omitted the energy dependence of eigenvalues and eigenvectors in (2.5), for sake of simplicity in the notation, and we have collectively denoted, respectively, with F and $\bar{F}$ the amplitudes corresponding to positive and negative RPA eigenstates. The solutions of (2.5) are denoted by $|\nu\rangle$, whereas the RPA basis vectors are labeled by $|n\rangle$, according to

$$|\nu\rangle = \sum_n F^{(\nu)}_n |n\rangle. \tag{2.6}$$

It is worthwhile at this point to notice that an approach based on TDA instead of RPA leads to an equation in which only the upper-left quarter of the matrix that appears in (2.5) is present. The matrix in (2.5) is complex symmetric as can be seen from its explicit form in Appendix A (see also [13]). The transformation which makes it diagonal, that is the matrix of its eigenvectors, is complex orthogonal, i.e.,

$$F^T F = F F^T = 1. \tag{2.7}$$

A useful quantity characterizing a mode excited by a given operator O is the response function,

$$R(\omega) = \langle 0|O^{\dagger} \frac{1}{\omega - \mathcal{H}(\omega) + i\epsilon} O|0\rangle. \tag{2.8}$$

The corresponding strength function is related to (2.8) by the well-known relation

$$S(\omega) = -\frac{1}{\pi}\mathrm{Im}R(\omega). \tag{2.9}$$

In terms of solutions of (2.5) the strength function is

$$S(\omega) = -\frac{1}{\pi}\mathrm{Im}\sum_\nu \langle 0|O|\nu\rangle^2 \frac{1}{\omega - \Omega_\nu + i\frac{\Gamma_\nu}{2}}, \tag{2.10}$$

where the squared matrix element of O appears, instead of its squared modulus, due to the properties of the eigenvectors $|\nu\rangle$, which form a biorthogonal basis. We stress at this point that, although not explicitly written, the eigenvalues labeled by ν as well as the wave functions needed to compute the matrix elements of O depend on ω, as the effective Hamiltonian does. So, better than the eigenvalue distribution, which can change when diagonalizing the effective Hamiltonian at different energies, the strength function really carries information about the couplings taken into account, and can be directly compared with experimental results. Note also that, when all the above scheme is carried out without Q_2 space, one should recover continuum-RPA results. It is this kind of consistency check that we alluded to in mentioning Figs. 1–3 of [14] and Fig. 1 of [16].

Another quantity which can be extracted from the model and which is actually measured in the particle decay experiments is the branching ratio B_c corresponding to a particular decay channel. An escaping nucleon with energy ε leaves a residual $(A-1)$ system in a hole state such that, by energy conservation $\varepsilon_h = \varepsilon - \omega$, where ω is the initial excitation energy. The cross section σ_c for this decay was calculated in [13] [see Eq. (3.40)], and a discussion is also given in [18] where a plane wave Born approximation (PWBA) is used to describe the reaction mechanism. In Appendix B we summarize this procedure and show how the same PWBA can lead from Eq. (3.38) of [13] to a more computable expression for the excitation cross section σ_{exc}. Using the results of Appendix B, the branching ratio comes out as

[2]These configurations display a rather high level-density in medium-heavy nuclei, of the order of 10^2–10^3 levels per MeV in the region of giant resonances if we think in terms of 2p-2h configurations [17], so that to calculate their mutual interaction would be a formidable task.

$$B_c(\omega) \equiv \frac{\sigma_c(\omega)}{\sigma_{\rm exc}(\omega)} = \frac{\sum_{\nu,\nu'} S_{\nu'\nu}\gamma_{\nu'\nu,c}(\omega - \Omega_\nu - i\frac{\Gamma_\nu}{2})^{-1}(\omega - \Omega_{\nu'} + i\frac{\Gamma_{\nu'}}{2})^{-1}}{-2{\rm Im}\sum_{\nu,\nu'} S_{\nu'\nu}(F^*F^T)_{\nu\nu'}(\omega - \Omega_{\nu'} - i\frac{\Gamma_{\nu'}}{2})^{-1}}, \tag{2.11}$$

where $S_{\nu\nu'}$ is given in (B6) and

$$\gamma_{\nu\nu',c} = \int d\Omega_k \gamma_{\nu,c}(\vec{k})\gamma^*_{\nu',c}(\vec{k}), \tag{2.12}$$

with

$$\gamma_{\nu,c}(\vec{k}) = \langle \varphi_c\, u^{(-)}_{c,\varepsilon}(\vec{k})|H_0|\nu\rangle. \tag{2.13}$$

In Eq. (2.13), φ_c is the wave function describing the residual $(A-1)$ nucleus in channel c, and $u^{(-)}_{c,\varepsilon}(\vec{k})$ is the escaping particle wave function belonging to P space. The strength functions and the branching ratios are the main quantities we are going to show as results of the present model and which can be directly confronted with experiment. Before coming to this, we add some important remarks relevant to calculations of charge-exchange resonances.

III. CALCULATION OF CHARGE-EXCHANGE RESONANCES

The model we have just presented was used in its TDA version and without the inclusion of the spreading term $W^\downarrow$ to calculate the IAR and GTR in ^{208}Bi [5]. Details about the HF and TDA procedures as well as the coupling with continuum configurations can be found in [5]. On the other hand, the inclusion of the spreading term is an improvement of the model. Moreover, this term was never included in previous calculations of the IAR in the form of coupling with collective vibrations, as it is done here. While coupling to collective vibrations has been used for the GTR (cf. [19, 20]), the IAR case has only been treated by using for $|N\rangle$ the 2p-2h configurations to build $W^\downarrow$ ([15, 17]). In the present work, we want to use the same model to construct the $W^\downarrow$ term for IAR and GTR, and therefore isospin conservation rules must be carefully treated as discussed at the end of this section.

We have consistently used the two interactions SIII and SGII throughout the whole procedure. The HF mean field for ^{208}Pb is diagonalized on a basis of 15 shells of the set of harmonic oscillator eigenfunctions with $\hbar\omega_0$=6.2 MeV (see also [21]). For the construction of subspace Q_1, the set $|i\rangle$ contains all occupied levels and Δn unoccupied proton levels for each value of (l, j). Δn is 6 in the IAR case, and 7 in the GTR case, as in [5]. The difference with this previous work is the inclusion in the present case of the Coulomb exchange term in the Slater approximation inside the HF mean field.

We have then performed a TDA calculation within Q_1, as the large neutron excess of ^{208}Pb should hinder ground-state correlations effects for proton particle-neutron hole configurations. This gives the basis of states $|n\rangle$ on which Eq. (2.5) is solved. We have built the configurations of subspace Q_2 by coupling a proton particle and a neutron hole in the discrete states of the set $|i\rangle$ with collective vibrations of the ^{208}Pb core. These doorway states, introduced above and labeled by $|N\rangle$ play an essential role in the damping of giant resonances. As pointed out in [9], the reason is that the choice of 2p-2h as doorway states amounts to neglect a number of correlations induced by the residual interaction V_{ph}. Many of these correlations are included if the low-lying collective vibrations are explicitly taken into account as doorway states.

The collective vibrations of the nucleus ^{208}Pb have been calculated in self-consistent RPA, with the same SIII or SGII interaction used throughout the whole work, in a way completely analogous to [22], where the coupling with collective vibrations was used to study the energies and spectroscopic factors of single-particle states. We refer then for details to [22], summarizing here the main points. We have built the complete spectra of isoscalar modes of J^π equal to 2^+, 3^-, and 4^+. In the configurations of Q_2, however, only states with more than 1% of the total EWSR, and with energy less than 20 MeV, were included. The low-lying 5^- state was also included, but its contribution was found negligible. The collective states included in the calculations with SIII have been shown in [22], and those corresponding to SGII are shown in Table I and compared with [23]. The limits in the accuracy with which this Skyrme-RPA calculation can reproduce the experimental findings are comparable to the case of similar calculations performed in the past decades. At this point we can build the matrix elements of the operator

$$W^\downarrow(\omega) = \sum_N \frac{V|N\rangle\langle N|V}{\omega - \omega_N}, \tag{3.1}$$

as in Eq. (2.4) (these are essential ingredients to build the matrix elements on TDA basis). $W^\downarrow_{ph,p'h'}$ of (2.4) is a sum of terms whose diagrammatic representation is shown in Fig. 1. To evaluate these diagrams an expression for the interaction vertices is needed. This is provided by the particle-vibration coupling model, by introducing a one-

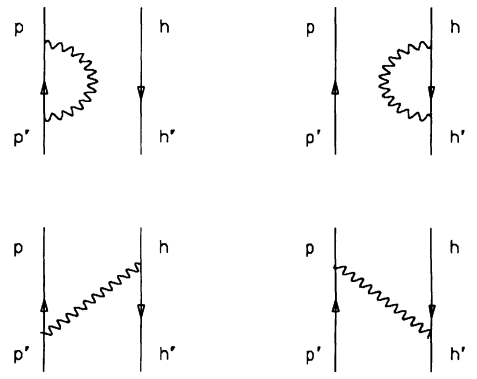

FIG. 1. Diagrammatic representation of the four terms whose sum gives the matrix element $W^\downarrow_{ph,p'h'}$ of (2.4). The analytic expressions are shown in Appendix A, Eq. (A12).

TABLE I. Vibrational states of ^{208}Pb, resulting from a coordinate-space RPA calculation employing the SGII force, with energy below $\sim$ 20 MeV, and exhausted percentage of EWSR larger than 1%. They are used to build the "doorway states," that is, the configurations which are more complicated than the 1p-1h configurations and therefore play a role in the damping process of giant resonances. The experimental values in this table are taken from [23].

	Theory			Experiment	
J^π	Energy [MeV]	$B(E\lambda)$ [spu]	Percentage of EWSR	Energy [MeV]	$B(E\lambda)$ [spu] (or percentage of EWSR)
2^+	4.78	3.28	7	4.085	6.2
	5.13	4.36	10	4.923	
				5.036	
				5.128	
	11.16	15.03	75	10.6	(%EWSR=70)
3^-	2.64	37.68	25	2.614	34.2
	13.6	0.62	1.6		
	14	0.37	1		
	16.53	0.41	1.3		
	17.55	0.30	1		
	18.17	0.40	1.4		
	20.68	10.13	40	20.9	(%EWSR=36)
4^+	4.82	2.52	1.1	4.323	23
	5.71	11.21	5.8	5.690	
	12.05	9.61	10.5	12.	(%EWSR=10)
	12.44	4.52	5.1		
	13.17	2.43	2.9		
	14.66	1.43	1.9		
	15.14	0.80	1.1		
5^-	3.58	16.37	2.6	3.198	17.4

body field which can be written in the form

$$V = \sum_{\alpha\beta} \sum_{LnM} \langle \alpha | \varrho_n^{(L)}(r) v(r) Y_{LM}(\hat{r}) | \beta \rangle \; a_\alpha^\dagger a_\beta. \quad (3.2)$$

In this equation, we have introduced the radial transition density $\varrho_n^{(L)}(r)$ of the $|n\rangle$ states of the spectrum of phonons with angular momentum L. This is defined in terms of the RPA states as

$$\langle n | \psi^\dagger(\vec{r}) \psi(\vec{r}) | 0 \rangle \equiv \varrho_n^{(L)}(r) Y_{LM}(\hat{r}), \quad (3.3)$$

where $\psi^\dagger(\vec{r})$ and $\psi(\vec{r})$ are the creation and annihilation operators of a nucleon at point $\vec{r}$, respectively. The form factor $v(r)$ appearing in (3.2) is related to the p-h interaction derived from the Skyrme force by $V_{ph}(\vec{r}_1, \vec{r}_2) = v(r_1)\delta(\vec{r}_1 - \vec{r}_2)$, as in [22]. Once all these starting points are given, the evaluation of the diagrams of Fig. 1 is straightforward and their detailed expressions are given in Appendix A.

Up to here, the procedure is the one already applied for the giant monopole resonance in [8]. Since we deal here with charge-exchange modes, it must be noted that the operator (3.1) can mix states with different isospins. The coupling (3.2) is manifestly a scalar in the total fermion-boson isospin space. But the intermediate states $|N\rangle$ do not have pure isospin, as they contain a proton particle and a neutron hole (see the diagrams of Fig. 1, where the phonons are isoscalar and therefore do not cause any change in the fermion isospin in the intermediate states, with respect to the initial state). This leads naturally to a coupling of the IAR, which has isospin quantum numbers $|T, T_z\rangle = |T_0, T_0 - 1\rangle$ where $T_0 = N - Z/2$, with states which in general have a mixture of different T components. The nuclear part of the Hamiltonian actually forbids this coupling, and we impose that it is strictly forbidden (this amounts to neglecting Coulomb effects in the residual interaction). This can be done by projecting out the T_0 component of the intermediate state $|N\rangle$. More precisely, we can write in isospin space

$$|N\rangle = c_{-1}|N;\ T_0 - 1, T_0 - 1\rangle + c_0 |N;\ T_0, T_0 - 1\rangle + c_{+1}|N;\ T_0 + 1, T_0 - 1\rangle, \quad (3.4)$$

and we define three projectors P_{-1}, P_0, and P_{+1} such that

$$P_i|N\rangle = c_i |N; T_0 + i, T_0 - 1\rangle, \quad -1 \le i \le 1. \quad (3.5)$$

The coefficients c_i are simply Clebsch-Gordan coefficients (we use the coupling $\{|1, -1\rangle |T_0, T_0\rangle\}_{T, T_0 - 1}$),

$$c_{-1} = +(2T_0 - 1)^{1/2}(2T_0 + 1)^{-1/2},$$
$$c_0 = -(T_0 + 1)^{-1/2},$$
$$c_{+1} = +(T_0 + 1)^{-1/2}(2T_0 + 1)^{-1/2}. \quad (3.6)$$

Similarly, the basis states of the Q_1 space can be decomposed into isospin components in the same way as Eq. (3.4), and one must select the component relevant to the case at hand. Therefore, in the IAR case the correct spreading operator having the right isospin structure is

$$W^{\downarrow}_{T_0}(\omega) = \sum_N \frac{VP_0|N\rangle\langle N|P_0V}{\omega - \omega_N}. \quad (3.7)$$

Actually, the matrix elements of this operator are simply proportional to those of (3.1), the multiplicative constant being $|c_0|^2 \equiv (T_0+1)^{-1}$. In the GTR case, we use the operator $W^{\downarrow}_{T_0-1}$ defined in a fully analogous way, and thus proportional to (3.1) by means of the constant $|c_{-1}|^2$.

This procedure allows us to respect isospin symmetry. A similar procedure was not necessary in the IAR calculations of [15] and [17], where the intermediate states $|N\rangle$ were chosen as 2p-2h configurations. The interaction V was the nuclear two-body interaction, and the approximation used corresponds to the well-known second RPA (SRPA). This automatically preserves the isospin structure, due to the respect of conservation laws in SRPA [24], and to the character of the interaction. On the other hand, an approach similar to ours has been used in [19,20] for the GTR without any isospin factor, i.e., with the spreading operator (3.1); as the correct one, $W^{\downarrow}_{T_0-1}$, differs by a factor $|c_{-1}|^2$ close to 1 in the case of ^{208}Pb, the numerical results are not markedly affected by this neglecting of isospin symmetry.

IV. ISOBARIC ANALOG RESONANCE RESULTS

The calculated strength distributions in the IAR region are shown in Figs. 2 (interaction SIII) and 3 (interaction SGII). Table II includes the main quantities which can be extracted from these strength distributions, that is centroid energy, width, and percentage of strength of the resonance. From the TDA calculation, a discrete state emerges which, in SIII and SGII case, respectively, lies at 18.59 or 18.54 MeV, and carries 86% or 87% of the total strength $(N-Z)$ of the operator $T_- \equiv \sum_{i=1}^{A} t_-(i)$. In fact, isospin is explicitly projected out only in the spreading term, whereas the TDA calculation is performed in a space with all isospin components included. Nevertheless, the strength relative to T_- operator selects as most collective state a single one, which was checked to be almost pure in isospin by looking at its T^2 expectation value. In Figs. 2 and 3 the dashed line corresponds to a calculation with $W^{\uparrow}$ only, and the full line to the complete calculation. We remark first that, in contrast with other modes where a certain amount of fragmentation is present, in this case this strength function is essentially due to a single state. The effect of $W^{\uparrow} + W^{\downarrow}$ is to shift slightly the peak energy and to produce a total width. With SIII, the peak is at 18.49 MeV and has a width of 152 keV whereas the corresponding values are 18.64 MeV and 99 keV with SGII. In both cases the state exhausts 97% of T_- strength. If one performs calculations with $W^{\uparrow}$ or $W^{\downarrow}$ only, one can obtain separately $\Gamma^{\uparrow}$ and $\Gamma^{\downarrow}$. We find that the sum $\Gamma^{\uparrow} + \Gamma^{\downarrow}$ is equal, within a few percent, to the total width in the complete calculation. It can be seen that this width is rather sensitive to the interaction used, since the width calculated with SIII is 50% larger than that of SGII.

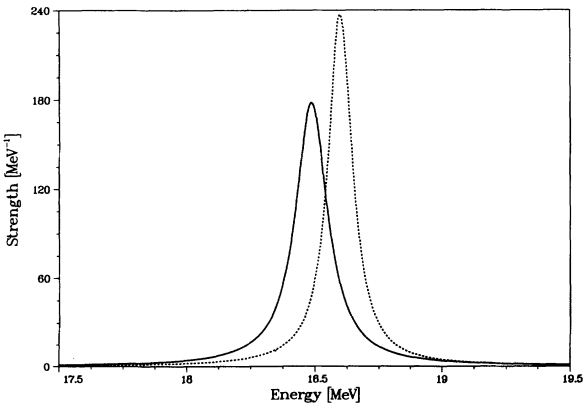

FIG. 2. Strength distribution of IAR in ^{208}Bi calculated with the interaction SIII. The full line refers to the complete calculation, whereas the dashed line gives the result with only the continuum coupling.

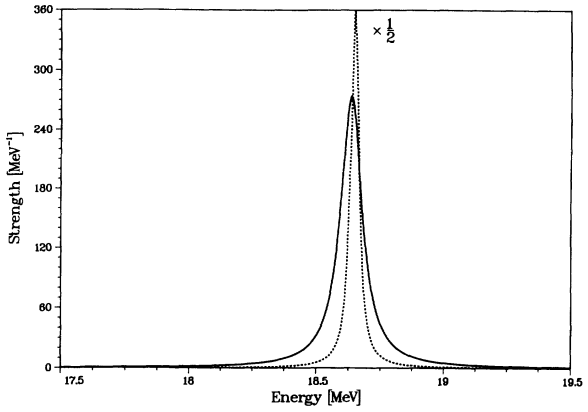

FIG. 3. Strength distribution of IAR in ^{208}Bi calculated with the interaction SGII and displayed as in Fig. 2.

The complex collective state, expanded on the TDA basis, shows a squared overlap of 0.90 (respectively 0.91) with the collective TDA state if one calculates with SIII (respectively SGII). We must also mention that the spreading term $W^{\downarrow}$ has been calculated with an averaging parameter $i\Delta$ added to the denominator of (3.7), for reason of convenience. This means that one makes a Lorentzian averaging of the distribution of intermediate states $|N\rangle$, with Δ corresponding to half of the Lorentzian width. The quantity Δ has been chosen to be 100 keV, but results are stable with respect to its variation, as doubling Δ implies an increase by only about 20 keV in the total width. Experimental values for IAR excitation energy and total width are, respectively, 18.8 MeV and 232 keV [25]. This state exhausts more or less the whole T_- strength.

Branching ratios corresponding to proton emission leaving the residual nucleus in a valence neutron hole state of ^{207}Pb are shown in Tables III and IV. In these tables, the column labeled "only $W^{\uparrow}$" refers to a calculation with only the escape included, and the results correspond to those of [5]. The other three columns under

TABLE II. Averaged quantities extracted from the strength distributions of IAR and GTR. In the case of IAR only one peak appears, as expected, and we display the energy, the full width and the percentage of strength under the peak. In the case of GTR we take into account the whole energy region $(E_<, E_>)$ in which bumps of the strength function are visible. The values of $E_<$ and $E_>$, as well as the definitions of the mean energy and width, are given in the text (Sec. V).

	Isobaric analog resonance		
	Theory		
	SIII	SGII	Experiment [25]
Mean energy	18.49 MeV	18.64 MeV	18.8 MeV
Width	152 keV	99 keV	232 keV
Percentage of strength	97%	97%	$\sim$ 100%
	Gamow-Teller resonance		
	Theory		
	SIII	SGII	Experiment [4]
Mean energy	21.11 MeV	22.43 MeV	19.2 MeV
Width	3 MeV	3.1 MeV	3.7 MeV
Percentage of strength	61%	68%	~60–70% [27]

"$W^{\uparrow} + W^{\downarrow}$" include the results of the complete calculation. Column (a) corresponds to the case where the final states are pure Hartree-Fock ones. These final states can be renormalized by means of energy and spectroscopic factors, either calculated with the same Skyrme force, and we have these values in the SIII case in [22] so we can show the corresponding results for the branching ratios in column (b), or taken from empirical estimates [26], and the branching ratios obtained in this way are shown in column (c). These calculated results are compared with the experimental values quoted in Ref. [4]. The agreement of the total sum of branching ratios with the experimental value in the SIII case and in column (b) is quite remarkable, as this is the most consistent fashion to perform a theoretical calculation. Minor discrepancies are found by looking in the same column at individual channels. On the other hand, calculated decay branching ratios depend sensitively on the Skyrme force employed, even when predicted peak energies and strengths are practically the same. By examining the IAR wave function obtained from our calculation, we have noticed that the p-h amplitudes corresponding to a change in the principal quantum number n are not negligible and this indicates that a simple picture of the IAR as given by a $T_-|0\rangle$ wave function is slightly too schematic, at least in the nucleus we have considered.

V. GAMOW-TELLER RESONANCE RESULTS

We follow a similar pattern in presenting the results for the GTR in ^{208}Bi. Figures 4 and 5 show the strength functions calculated, respectively, with SIII and SGII interactions and Table II includes centroids, widths, and percentages of strength of these distributions. With SIII, at least two main states contribute: besides the main bump at about 21.50 MeV, a smaller one appears at lower energy. In the case of SGII, there are two smaller bumps in addition to the main one at about 23 MeV. One can understand this broadened line shape by looking at the underlying complex states coming out of the diagonalization of the effective Hamiltonian (2.2). There are several important complex states spread over the energy interval 18–25 MeV. This is in contrast with the IAR case and it can be understood by relating to the

TABLE III. Branching ratios for the proton decay of IAR in ^{208}Bi to neutron valence hole states of ^{207}Pb, obtained by using the SIII force. In column (a) the final state is a pure HF configuration, whereas in other columns its energy and wave function are corrected either by means of a consistent SIII calculation (b) or by using empirical values (c).

	Theory				
Decay	Only $W^{\uparrow}$	$W^{\uparrow} + W^{\downarrow}$			Experiment
channel		(a)	(b)	(c)	[4]
$p_{1/2}$	0.472	0.346	0.253	0.237	0.22±0.02
$p_{3/2}$	0.396	0.287	0.238	0.196	0.34±0.04
$i_{13/2}$	0.015	0.011	0.008	0.010	-
$f_{5/2}$	0.117	0.086	0.065	0.061	included in $p_{3/2}$
$f_{7/2}$	$< 10^{-3}$	$< 10^{-3}$	$< 10^{-3}$	$< 10^{-3}$	0.015±0.007
$h_{9/2}$	$< 10^{-3}$	$< 10^{-3}$	$< 10^{-3}$	$< 10^{-3}$	-
$\sum_c B_c$	1.0	0.730	0.564	0.504	0.575±0.07

TABLE IV. Same as Table III, in the case of the SGII force.

Decay channel	Theory: Only $W^{\uparrow}$	Theory: $W^{\uparrow}+W^{\downarrow}$ (a)	Theory: $W^{\uparrow}+W^{\downarrow}$ (c)	Experiment [4]
$p_{1/2}$	0.448	0.171	0.137	0.22±0.02
$p_{3/2}$	0.514	0.198	0.157	0.34±0.04
$i_{13/2}$	0.016	0.007	0.006	-
$f_{5/2}$	0.016	0.008	0.006	includ. in $p_{3/2}$
$f_{7/2}$	0.006	0.002	0.004	0.015±0.007
$h_{9/2}$	$< 10^{-3}$	$< 10^{-3}$	$< 10^{-3}$	-
$\sum_c B_c$	1.0	0.386	0.310	0.575±0.07

larger density of $T_0 - 1$ states compared to that of T_0 states, in this energy region of the ^{208}Bi spectrum. The effect of $W^{\downarrow}$ coupling is much stronger for GTR and consequently it admixes TDA states more than for IAR. The percentage of the total strength of the GTR operator $\beta_- = \frac{1}{2}\sum_{\mu=0,\pm1}\sum_{i=1}^{A}\sigma_\mu(i)\tau_-(i)$ [the so-called Ikeda sum rule, equal to $3(N-Z)$], is about 61% in the energy region 18–24 MeV for SIII, and about 68% in the interval 19.5–24.5 MeV, for SGII. This contrasts with the calculation with continuum only, where about the same fraction of strength is exhausted by the main narrower peak. In the complete calculation the remaining strength is found outside the forementioned interval $(E_<, E_>)$ and is rather fragmented. Experimentally, the strength concentrated in the GTR peak is about 50% of the total but this percentage rises up to about 60–70% if the whole energy region with some strength around the main bump is considered [27]. All the present theoretical results were calculated with an averaging parameter Δ equal to 250 keV. Again, the stability of the results has been checked by varying Δ.

Besides the peak energy, we can extract from the strength distribution a mean energy, given by

$$\langle\omega\rangle = \frac{\int_{E_<}^{E_>} d\omega\ \omega S(\omega)}{\int_{E_<}^{E_>} d\omega\ S(\omega)}, \tag{5.1}$$

and this turns out to be 21.11 MeV (SIII) or 22.43 MeV (SGII). Both values of $\langle\omega\rangle$ are somewhat larger than the experimental excitation energy of GTR which is 15.6 MeV in ^{208}Bi, corresponding to 19.2 MeV with respect to the ^{208}Pb ground state[3]. As for the width, the FWHM is not well defined in this case due to the double or triple peak. If we extract a value for the variance σ from the strength distribution, by defining

$$\sigma^2 = \frac{\int_{E_<}^{E_>} d\omega\ (\omega - \langle\omega\rangle)^2 S(\omega)}{\int_{E_<}^{E_>} d\omega\ S(\omega)}, \tag{5.2}$$

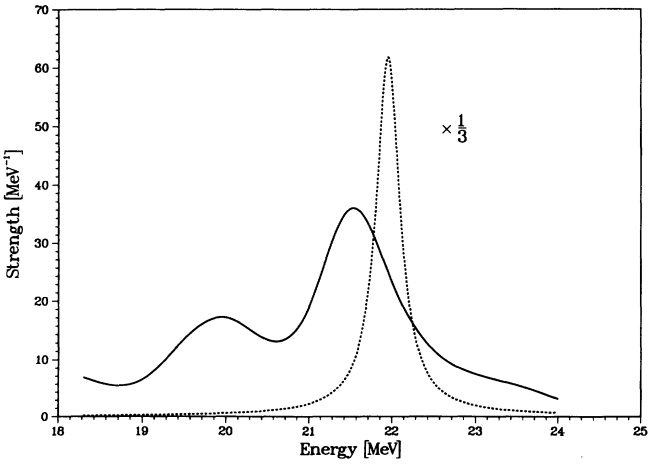

FIG. 4. Strength distribution of GTR in ^{208}Bi calculated with the interaction SIII. The two lines have the same meaning as in the case of IAR.

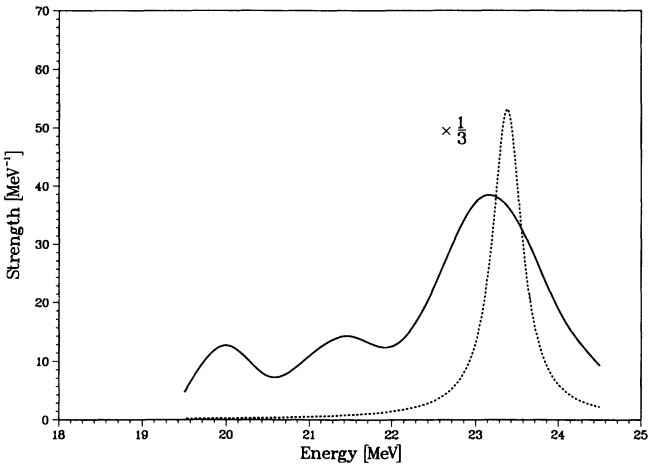

FIG. 5. Strength distribution of GTR in ^{208}Bi calculated with the interaction SGII and displayed as in Fig. 4.

[3]In order to reach this value, we have to add to the 15.6 MeV the mass difference between the two Bi and Pb isotopes, as well as the mass difference between neutron and proton which is missing when the GTR is built on the basis of p-h excitations.

TABLE V. Branching ratios for the proton decay of GTR in ^{208}Bi, obtained by using the SIII force. In column (a) the final state is a HF configuration. In column (b) we present the results of a calculation where the energy of the final neutron hole state is corrected in such a way the escaping particle has the same energy as in the experiment [4], and spectroscopic factors [26] are used.

Decay channel	Theory			Experiment
	Only $W^{\uparrow}$	$W^{\uparrow}+W^{\downarrow}$		
		(a)	(b)	[4]
$p_{1/2}$	0.265	0.037	0.022	0.013±0.002
$p_{3/2}$	0.432	0.055	0.033	0.023±0.003
$i_{13/2}$	0.009	0.001	0.001	0.002±0.002
$f_{5/2}$	0.278	0.051	0.030	included in $p_{3/2}$
$f_{7/2}$	0.011	0.009	0.005	0.003±0.002
$h_{9/2}$	0.005	0.001	0.001	-
$\sum_c B_c$	1.0	0.154	0.092	0.041±0.009

we obtain a full width in Gaussian approximation ($\Gamma = 2.4\sigma$) of about 3 MeV for both interactions (slightly larger for SGII), to be compared with an experimental value of 3.8 MeV [4]. Of course, a model in which only the simplest class of "doorway states" is considered and not their full hierarchy, cannot but underestimate the width. The same model seems to predict correctly the giant monopole width [8] which is mainly due to Landau damping.

The overestimation of the peak energy, and the missing part of the damping effect, is probably the cause of a result for the branching ratios which correspond to a higher yield than the experimental one, as shown in Tables V and VI. Here, as the strength is spread over several MeV, we cannot calculate the branching ratios at a definite energy, as it was done for IAR, and we rather make an average over the energy interval $(E_<, E_>)$ of the numerator and denominator of (2.11):

$$B_c(\mathrm{GTR}) \equiv \frac{\langle \sigma_c \rangle}{\langle \sigma_{\mathrm{exc}} \rangle}. \tag{5.3}$$

Tables V and VI are displayed similarly to Tables III and IV except for the column (b) of the theoretical findings which we discuss below. First, one can notice that the discrepancy with experiment is reduced when going from self-consistent continuum RPA (column "only $W^{\uparrow}$") to the complete model. The results of SGII are in reasonable agreement with the data. We must also mention that preliminary indications from the MSU experiment [7] leave open the possibility that experimental branching ratios might be larger than found in [4]. On the other hand, the sensitivity of predictions with respect to the choice of the interaction is still present. We also show in column (b) of Tables V and VI what the proton yield would be, if the excitation energy corresponded to the experimental one (19.2 MeV). The branching ratios of column (b) have indeed been obtained by calculating the escape amplitudes (2.13) with the experimental outgoing proton energies ε. The empirical spectroscopic factors [26] already used in the case of IAR are also included. This renormalization obviously decreases the branching ratios and they are in good agreement with experiment in the case of SGII force. The final difference between theory and experiment, in the case of SIII force, is of the same order, or even smaller than the one found in the case of the giant monopole resonance [8], and simply indicates once more the limit one could expect in this kind of detailed study, due to the present uncertainty in the nuclear dynamics at low energy.

TABLE VI. Same as Table V, in the case of SGII force.

Decay channel	Theory			Experiment
	Only $W^{\uparrow}$	$W^{\uparrow}+W^{\downarrow}$		
		(a)	(b)	[4]
$p_{1/2}$	0.223	0.033	0.018	0.013±0.002
$p_{3/2}$	0.418	0.035	0.019	0.023±0.003
$i_{13/2}$	0.014	0.003	0.001	0.002±0.002
$f_{5/2}$	0.319	0.013	0.007	included in $p_{3/2}$
$f_{7/2}$	0.016	0.010	0.003	0.003±0.002
$h_{9/2}$	0.010	0.001	$< 10^{-3}$	
$\sum_c B_c$	1.0	0.095	0.048	0.041±0.009

We can finally compare our results obtained without the spreading terms with those of Muraviev and Urin [6] which are calculated in a continuum-RPA approach, where phenomenological inputs for the mean field and residual interaction are used. The large differences between the two sets of results cannot be explained by invoking the approximation made in the present work in treating the single-particle continuum, as already discussed after Eq. (2.3). It should be attributed to the sensitivity of branching ratios to the details of the inputs. As we have seen here differences in results coming from the same model but using two different Skyrme interactions, it is not too surprising that results from phenomenological RPA calculations, based on a Woods-Saxon potential and a residual interaction of the Landau-Migdal type can also differ. A similar situation also exists in the giant monopole resonance case [28].

VI. CONCLUSIONS

Within linear response theory, a microscopic model of collective excitations based on RPA states coupled to doorway states composed of 1p-1h configurations plus a collective vibration, and to 1p-1h continuum states has

been applied to the study of the properties of two important charge-exchange modes, the IAR and GTR in ^{208}Bi. The two types of coupling are intended to describe the essential physical mechanisms leading to the spreading of the collective mode and its decay by nucleon emission. The model contains no free parameter but depends on the choice of the effective nucleon-nucleon interaction.

The physical quantities which can be calculated are the strength distributions and the cross sections of nucleon decay into various channels. From these quantities centroid energies, widths, and particle decay branching ratios are obtained. The calculated results show some sensitivity to the choice of the effective interaction.

In the IAR case, both SIII and SGII interactions predict the correct peak energy, and SIII gives a good description of the data for the decay branching ratios whereas SGII tends to underestimate the branching ratios as well as the total width.

For the GTR, interactions SIII and SGII overestimate the mean energy, respectively, by 2 and 3 MeV, while they both predict a total width of about 3 MeV, i.e., 75% of the experimental value. Looking at branching ratios, it appears that SGII comes very close to experiment if one corrects for the overestimate of the GTR energy. The discrepancy with experimental values (in the case of SIII) is of the same order or even smaller than that already found in the case of the isoscalar monopole resonance using the same model. This level of agreement with experiment indicates the present limits of existing Skyrme effective interactions.

ACKNOWLEDGMENTS

One of the authors (G.C.) would like to gratefully acknowledge the support of ECT*, the continuous interest of R. Leonardi and the useful discussions with D.M. Brink, in the period November 1993–January 1994, during which a part of the present work was carried out. The financial support from the European Community (Contract No. CHRXCT92-0075) is gratefully acknowledged.

APPENDIX A: MATRIX ELEMENTS OF THE EFFECTIVE HAMILTONIAN

We show in this Appendix how to evaluate matrix elements of the escape and spreading terms $W^{\uparrow}$ and $W^{\downarrow}$ of the effective Hamiltonian (2.2), on a RPA or TDA basis. We consider explicitly the RPA case, as the reduction to TDA comes out quite transparently. First we suppose that the effective Hamiltonian *contains only the RPA and the escape term*, and we derive the explicit form of Eq. (2.5) in this case. Then, we show how the spreading term can be taken into account.

We denote a generic element of the RPA basis by $|n\rangle$, its energy being ω_n. Another state with energy $-\omega_n$ is present in the basis (see chapter 14 of [29]), and we denote it by $|\bar{n}\rangle$. The creation operators of these states are, respectively, $O_n^\dagger$ and $\bar{O}_n^\dagger$. The creators $\mathcal{O}_\nu^\dagger$ of the states $|\nu\rangle$, resulting from the diagonalization of the effective Hamiltonian (2.2), can be expressed as a linear combination of the RPA creators, since these are a complete set in Q_1,

$$\mathcal{O}_\nu^\dagger = \sum_{\omega_n>0} F_n^{(\nu)} O_n^\dagger - \bar{F}_n^{(\nu)} \bar{O}_n^\dagger, \tag{A1}$$

where the amplitudes F and $\bar{F}$ are in general complex numbers.

The eigenvalue equation for the effective Hamiltonian is

$$\left[\mathcal{H}, \mathcal{O}_\nu^\dagger\right] = \left(\Omega_\nu - i\frac{\Gamma_\nu}{2}\right) \mathcal{O}_\nu^\dagger, \tag{A2}$$

where we have fixed at a definite value the energy at which the effective Hamiltonian must be evaluated, and omitted to indicate explicitly this energy dependence. Using the property

$$\left[Q_1 H Q_1, O_n^\dagger\right] = \omega_n O_n^\dagger, \tag{A3}$$

(a minus sign appears in the right-hand side if we consider $\bar{O}_n^\dagger$), we obtain

$$\sum_{\omega_n>0} F_n^{(\nu)}(\omega_n O_n^\dagger + [W^{\uparrow}, O_n^\dagger]) - \bar{F}_n^{(\nu)}(-\omega_n \bar{O}_n^\dagger + [W^{\uparrow}, \bar{O}_n^\dagger])$$
$$= \left(\Omega_\nu - i\frac{\Gamma_\nu}{2}\right) \sum_{\omega_n>0} F_n^{(\nu)} O_n^\dagger - \bar{F}_n^{(\nu)} \bar{O}_n^\dagger. \tag{A4}$$

If we take the expectation values of (A4), first between $\langle 0|O_m$ and $|0\rangle$, then between $\langle 0|\bar{O}_m$ and $|0\rangle$, we build a set of $2n_>$ equations ($n_>$ is the number of positive RPA eigenvalues) whose matrix form is the one of (2.5).

In (2.5) each submatrix has dimension $n_>$. The submatrix $\mathcal{D}$ is diagonal and contains the contribution of the term $Q_1 H Q_1$ of (2.2),

$$\mathcal{D}_{mn} = \delta_{mn}\omega_n. \tag{A5}$$

The contributions to the submatrices $\mathcal{A}_i$ coming from the escape term are given by

$$(\mathcal{A}_1)_{mn}^{\rm esc} = \langle 0|\left[O_m, [W^{\uparrow}, O_n^\dagger]\right]|0\rangle,$$
$$(\mathcal{A}_2)_{mn}^{\rm esc} = -\langle 0|\left[O_m, [W^{\uparrow}, \bar{O}_n^\dagger]\right]|0\rangle,$$
$$(\mathcal{A}_3)_{mn}^{\rm esc} = \langle 0|\left[\bar{O}_m, [W^{\uparrow}, O_n^\dagger]\right]|0\rangle,$$
$$(\mathcal{A}_4)_{mn}^{\rm esc} = -\langle 0|\left[\bar{O}_m, [W^{\uparrow}, \bar{O}_n^\dagger]\right]|0\rangle. \tag{A6}$$

To work out explicitly these matrix elements we approximate $W^{\uparrow}$ with expression (2.3) (see the discussion in Sec. II about this point).

The operator K which appears in (2.3) satisfies (as said in Sec. II but see also [13]) the following equation,

$$K \cdot Q_1 \frac{1}{\omega - H_0 + i\epsilon} Q_1 = Q_1. \tag{A7}$$

The propagator $\frac{1}{(\omega - H_0 + i\epsilon)^{-1}}$ can be expanded in its partial wave components labeled by (l,j), and each component $g_{lj}(r_1,r_2)$ is written by means of the regular and irregular solutions [$f_{lj}(r)$ and $g_{lj}(r)$] of the corresponding radial Schrödinger equation with energy ω,

$$g_{lj}(r_1,r_2) = -\frac{2m^*}{\hbar^2} f_{lj}(r_<) g_{lj}(r_>) \cdot W^{-1}, \tag{A8}$$

where m^* is the nucleon effective mass, $r_>$ ($r_<$) are the

larger (the smaller) between r_1 and r_2, and W is the Wronskian of f_{lj} and g_{lj} [30]. In this form the propagator is more easily inverted to obtain K. This is a p-h operator diagonal in the hole and for a given hole h we label as K_h the corresponding particle operator.

The matrix elements of the escape term are then written in terms of the ones of K_h and of the RPA amplitudes $X_{ph}^{(n)}$ and $Y_{ph}^{(n)}$ as

$$
\begin{aligned}
(\mathcal{A}_1)_{mn}^{\rm esc} &= -\sum_{ph}(\varepsilon_p-\varepsilon_h)(X_{ph}^{(m)}X_{ph}^{(n)}+Y_{ph}^{(m)}Y_{ph}^{(n)})-\sum_{ph,p'h'}\langle p'|K_h|p\rangle\delta_{hh'}(X_{p'h'}^{(m)}X_{ph}^{(n)}+Y_{p'h'}^{(m)}Y_{ph}^{(n)}),\\
(\mathcal{A}_2)_{mn}^{\rm esc} &= \sum_{ph,p'h'}[(\varepsilon_p-\varepsilon_h)\delta_{pp'}\delta_{hh'}+\langle p'|K_h|p\rangle\delta_{hh'}](X_{p'h'}^{(m)}Y_{ph}^{(n)}+Y_{p'h'}^{(m)}X_{ph}^{(n)}),\\
(\mathcal{A}_3)_{mn}^{\rm esc} &= (\mathcal{A}_2)_{mn}^{\rm esc},\\
(\mathcal{A}_4)_{mn}^{\rm esc} &= (\mathcal{A}_1)_{mn}^{\rm esc}.
\end{aligned}
\tag{A9}
$$

We now turn to the calculation of the *spreading* term. It is known (see, e.g., the first chapter of [11]) that diagonalizing an effective Hamiltonian including this term besides the RPA one, and with a set of 2p-2h configurations in the Q_2 space, amounts to solve

$$
\begin{pmatrix} A+W^{\downarrow}(\omega) & B \\ -B^* & -A^*-W^{\downarrow *}(-\omega)\end{pmatrix}\begin{pmatrix} X \\ Y\end{pmatrix}=\omega\begin{pmatrix} X \\ Y\end{pmatrix},
\tag{A10}
$$

where A and B are the RPA matrices and $W^{\downarrow}$ has the matrix elements defined by (2.4). Equation (A10) is the eigenvalue problem in the SRPA scheme mentioned in the text. A similar pattern holds even if a different choice of Q_2 is made,[4] like in the present case, and therefore, in order to obtain the spreading matrix elements which must be inserted in (2.5) one has to transform the spreading part of Eq. (A10) which is written on the p-h basis of Q_1, and write it on the RPA basis.

The result is the spreading contribution to (2.5), which reads

$$
\begin{aligned}
(\mathcal{A}_1)_{mn}^{\rm spr} &= \sum_{ph,p'h'}W_{ph,p'h'}^{\downarrow}(\omega)X_{ph}^{(m)}X_{p'h'}^{(n)}+W_{ph,p'h'}^{\downarrow *}(-\omega)Y_{ph}^{(m)}Y_{p'h'}^{(n)},\\
(\mathcal{A}_2)_{mn}^{\rm spr} &= \sum_{ph,p'h'}W_{ph,p'h'}^{\downarrow}(\omega)X_{ph}^{(m)}Y_{p'h'}^{(n)}+W_{ph,p'h'}^{\downarrow *}(-\omega)Y_{ph}^{(m)}X_{p'h'}^{(n)},\\
(\mathcal{A}_3)_{mn}^{\rm spr} &= \sum_{ph,p'h'}W_{ph,p'h'}^{\downarrow}(\omega)Y_{ph}^{(m)}X_{p'h'}^{(n)}+W_{ph,p'h'}^{\downarrow *}(-\omega)X_{ph}^{(m)}Y_{p'h'}^{(n)},\\
(\mathcal{A}_4)_{mn}^{\rm spr} &= \sum_{ph,p'h'}W_{ph,p'h'}^{\downarrow}(\omega)Y_{ph}^{(m)}Y_{p'h'}^{(n)}+W_{ph,p'h'}^{\downarrow *}(-\omega)X_{ph}^{(m)}X_{p'h'}^{(n)}.
\end{aligned}
\tag{A11}
$$

The matrix elements $W_{ph,p'h'}^{\downarrow}$ can be evaluated as discussed in Sec. II. We give here their final expressions,

$$
\begin{aligned}
W_{ph,p'h'}^{\downarrow} &= \sum_{k=1}^{4}W^{\downarrow}(k),\\
W^{\downarrow}(1) &= \delta_{h,h'}\delta_{j_p,j_{p'}}\sum_{L,n,p''}\frac{1}{\omega-(\omega_n+\varepsilon_{p''}-\varepsilon_h)+i\Delta}\cdot\frac{|\langle j_p\|Y_L\|j_{p''}\rangle|^2}{\hat{j}_p^2}\\
&\quad\times\int dr_1u_{p'}(r_1)u_{p''}(r_1)v(r_1)\varrho_n^{(L)}(r_1)\int dr_3u_p(r_3)u_{p''}(r_3)v(r_3)\varrho_n^{(L)}(r_3),\\
W^{\downarrow}(2) &= \delta_{p,p'}\delta_{j_h,j_{h'}}\sum_{L,n,h''}\frac{1}{\omega-(\omega_n-\varepsilon_{h''}+\varepsilon_p)+i\Delta}\cdot\frac{|\langle j_h\|Y_L\|j_{h''}\rangle|^2}{\hat{j}_h^2}\\
&\quad\times\int dr_2u_{h'}(r_2)u_{h''}(r_2)v(r_2)\varrho_n^{(L)}(r_2)\int dr_4u_h(r_4)u_{h''}(r_4)v(r_4)\varrho_n^{(L)}(r_4),
\end{aligned}
$$

[4]The eigenvalue problem has the same form but not all the statements about SRPA contained e.g., in [24] are, strictly speaking, still valid.

$$W^{\downarrow}(3)=\sum_{L,n}\frac{(-1)^{1+j_{p'}+j_{h'}+L+J}}{\omega-(\omega_n+\varepsilon_p-\varepsilon_{h'})+i\Delta}\begin{Bmatrix} j_p & j_h & J \\ j_{h'} & j_{p'} & L\end{Bmatrix}\langle j_p\|Y_L\|j_{p'}\rangle\langle j_{h'}\|Y_L\|j_h\rangle$$
$$\times\int dr_1 u_p(r_1)u_{p'}(r_1)v(r_1)\varrho_n^{(L)}(r_1)\int dr_4 u_h(r_4)u_{h'}(r_4)v(r_4)\varrho_n^{(L)}(r_4),$$

$$W^{\downarrow}(4)=\sum_{L,n}\frac{(-1)^{1+j_{p'}+j_{h'}+L+J}}{\omega-(\omega_n+\varepsilon_{p'}-\varepsilon_h)+i\Delta}\begin{Bmatrix} j_p & j_h & J \\ j_{h'} & j_{p'} & L\end{Bmatrix}\langle j_p\|Y_L\|j_{p'}\rangle\langle j_{h'}\|Y_L\|j_h\rangle$$
$$\times\int dr_2 u_p(r_2)u_{p'}(r_2)v(r_2)\varrho_n^{(L)}(r_2)\int dr_3 u_h(r_3)u_{h'}(r_3)v(r_3)\varrho_n^{(L)}(r_3), \tag{A12}$$

where the symbol $\hat{j}$ denotes $(2j+1)^{1/2}$.

APPENDIX B: DECAY BRANCHING RATIOS

In [13] the cross sections σ_c and $\sigma_{\rm exc}$ (see Sec. II) are defined as

$$\sigma_c(\omega)=\frac{(2\pi)^3}{k^2}\sum_{\nu\nu'}T^*_{\nu 0}T_{\nu' 0}\gamma_{\nu'\nu,c}\left(\omega-\Omega_\nu-i\frac{\Gamma_\nu}{2}\right)^{-1}\left(\omega-\Omega_{\nu'}+i\frac{\Gamma_{\nu'}}{2}\right)^{-1},$$
$$\sigma_{\rm exc}(\omega)=-\frac{1}{\pi}\frac{(2\pi)^4}{k^2}{\rm Im}\sum_{\nu\nu'}T^*_{\nu 0}(F^*F^T)_{\nu\nu'}\left(\omega-\Omega_{\nu'}-i\frac{\Gamma_{\nu'}}{2}\right)^{-1}T_{\nu' 0}, \tag{B1}$$

where all the quantities are defined in the text, apart from k which is here the wave vector corresponding to the initial state of the projectile and the elements of the T matrix, in which one state is the initial state of target (labeled by 0). These matrix elements are (see also [13])

$$T_{\nu 0}=\langle\chi_f^{(-)}\Phi_\nu|V|\Phi_0\chi_i^{(+)}\rangle, \tag{B2}$$

where the initial and final wave functions of the projectile and ejectile are indicated by χ and those of the target nucleus by Φ. Here, V is an effective projectile-target interaction. We consider for our present purposes its $\vec{\tau}\cdot\vec{\tau}$ ($\vec{\sigma}\cdot\vec{\sigma}\vec{\tau}\cdot\vec{\tau}$) channel for the case of IAR (GTR) excitation. Either of these operators is labeled by O, so the interaction is $V_O(\vec{r}_1\cdots\vec{r}_A;\vec{r}_p)\cdot O$ where $\vec{r}_p$ is the projectile spatial coordinate. We are in the present work *not* interested in the reaction mechanism, provided it can excite the target in a state with definite quantum numbers. Therefore, we can make simplifications about this mechanism and we use standard PWBA methods to evaluate the element (B2). Plane wave functions are substituted to the initial and final wave functions of the projectile and ejectile, and an effective factor K takes care of the reduction of the reaction probability due to distortion which would come from a realistic estimate made by using an optical potential. In a straightforward way (B2) becomes

$$T_{\nu 0}=K\ \tilde{V}_O(\vec{q})\langle\nu|e^{\frac{i}{\hbar}\vec{q}\cdot\vec{r}}\cdot O|0\rangle, \tag{B3}$$

where $\vec{q}$ is the momentum transferred by the projectile and $\tilde{V}(\vec{q})$ is the Fourier transform of the interaction V_0. The exponential function can be decomposed as usual,

$$e^{i\vec{q}\cdot\vec{r}}=\sqrt{4\pi}\sum_{\lambda=0}^{\infty}i^\lambda\sqrt{2\lambda+1}\cdot j_\lambda(qr)Y_{\lambda 0}(\hat{r}), \tag{B4}$$

using Bessel functions and spherical harmonics. If we restrict to the λ value under consideration (0 as both IAR and GTR have no change of angular momentum with respect to the ground state in the space part of their wave function) and truncate the expansion of the Bessel function at the lowest order (low momentum transfer approximation), we obtain from (B4) a constant which can be included in the definition of $\tilde{V}$. Finally we are left with the approximate expression

$$T_{\nu 0}\sim{\rm const}\langle\nu|O|0\rangle. \tag{B5}$$

If we use this expression it is easy to show that the branching ratio, i.e., the ratio between the two cross sections defined in (B1), is given by (2.11) where

$$S_{\nu\nu'}\equiv\langle\nu|O|0\rangle\langle\nu'|O|0\rangle^*, \tag{B6}$$

and the other quantities are defined in Sec. II.

[1] K. Ikeda, S. Fujii, and J.I. Fujita, Phys. Lett. **3**, 271 (1963); J.I. Fujita and K. Ikeda, Nucl. Phys. **67**, 145 (1965).
[2] C. Gaarde, J. Rapaport, T.N. Taddeucci, C.D. Goodman, C.C. Foster, D.E. Bainum, C.A. Goulding, M.B. Greenfield, D.J. Horen, and E. Sugarbaker, Nucl. Phys. **A369**, 258 (1981), and references therein.
[3] C. Gaarde, J.S. Larsen, A.G. Drentje, M.N. Harakeh, and

S.Y. van der Werf, Phys. Rev. Lett. **46**, 902 (1981).
[4] H. Akimune, M. Yosoi, I. Daito, M. Fujiwara, T. Inomata, Y. Sakemi, Y. Fujita, M.B. Greenfield, M.N. Harakeh, J. Jänecke, K. Katori, S. Nakayama, H. Sakai, and M. Tanaka, Phys. Lett. B **323**, 107 (1994).
[5] N. Van Giai, P.F. Bortignon, A. Bracco, and R.A. Broglia, Phys. Lett. B **233**, 1 (1989).
[6] S.E. Muraviev and M.H. Urin, Nucl. Phys. **A569**, 267c (1994); to be published.
[7] S. Galès, private communication.
[8] G. Colò, P.F. Bortignon, N. Van Giai, A. Bracco, and R.A. Broglia, Phys. Lett. B **276**, 279 (1992).
[9] G.F. Bertsch, P.F. Bortignon, and R.A. Broglia, Rev. Mod. Phys. **55**, 287 (1983).
[10] S. Yoshida, Suppl. Progr. Theor. Phys. **74&75**, 142 (1983).
[11] *Electric and Magnetic Giant Resonances in Nuclei*, edited by J. Speth (World Scientific, Singapore, 1991).
[12] D. Vautherin and D.M. Brink, Phys. Rev. C **5**, 626 (1972); M. Beiner, H. Flocard, N. Van Giai, and P. Quentin, Nucl. Phys. **A238**, 29 (1975).
[13] S. Yoshida and S. Adachi, Z. Phys. **A325**, 441 (1986).
[14] S. Yoshida and S. Adachi, Nucl. Phys. **A457**, 84 (1986).
[15] S. Adachi and S. Yoshida, Nucl. Phys. **A462**, 61 (1987).
[16] N. Van Giai, P.F. Bortignon, F. Zardi, and R.A. Broglia, Phys. Lett. B **199**, 155 (1987).
[17] B. Schwesinger and J. Wambach, Nucl. Phys. **A426**, 253 (1984).
[18] F. Zardi, P.F. Bortignon, N. Van Giai, and R.A. Broglia, in *Proceedings of the 5th International Conference on Nuclear Reaction Mechanisms, Varenna, 1988*, edited by E. Gadioli (Università degli Studi di Milano Ricerca Scientifica ed Educazione Permanente), Vol. 66, p. 454.
[19] H.R. Fiebig and J. Wambach, Nucl. Phys. **A386**, 381 (1982).
[20] P.F. Bortignon, F. Zardi, and R.A. Broglia, in *Proceedings of the International Conference on Spin Excitations in Nuclei, Telluride, 1982*, edited by F. Petrovich *et al.* (Plenum Press, New York, 1984), p. 425.
[21] J.P. Blaizot and D. Gogny, Nucl. Phys. **A284**, 429 (1977).
[22] V. Bernard and N. Van Giai, Nucl. Phys. **A348**, 75 (1980).
[23] M.J. Martin, Nucl. Data Sheets, **47**, 797 (1986).
[24] C. Yannouleas, Phys. Rev. C **35**, 1159 (1987).
[25] R. Melzer, P. von Brentano, and H. Paetz gen. Schiek, Nucl. Phys. **A432**, 363 (1985).
[26] C. Mahaux and R. Sartor, Adv. Nucl. Phys. **20**, 1 (1991).
[27] C. Gaarde, in *Proceedings of the Niels Bohr Centennial Conference on Nuclear Structure*, edited by R.A. Broglia *et al.* (North-Holland, Amsterdam, 1985), p. 449c.
[28] A. Bracco, J.R. Beene, N. Van Giai, P.F. Bortignon, F. Zardi, and R.A. Broglia, Phys. Rev. Lett. **60**, 2603 (1988).
[29] D.J. Rowe, *Nuclear Collective Motion* (Methuen, London, 1970).
[30] K.F. Liu and N. Van Giai, Phys. Lett. **65B**, 23 (1976).